POLITECNICO
MILANO 1863

SCUOLA DI INGEGNERIA INDUSTRIALE
E DELL'INFORMAZIONE

Executive Summary of the Thesis

Depth Sensitivity in Diffuse Raman Spectroscopy based on a Time Domain Compressive Sensing approach

Laurea Magistrale in Physics Engineering - Ingegneria Fisica

Author: Valerio Gandolfi

Advisor: Prof. Antonio Giovanni Pifferi

Co-advisors: Dr. Alessandro Bossi, Prof. Fabrizio Martelli

Academic year: 2021-2022

1. Introduction

In many fields, from biomedicine to industry and material research, the problem of analyzing the chemical composition of deep layers of a sample is often encountered and sometimes also a quantification of the analyzed depth is required.
Diffuse Raman spectroscopy (DIRS), a recently growing technique which unifies the chemical specificity of Raman Spectroscopy and the penetration depth of Diffuse Optics, allows solving this problem. In fact, it has been already demonstrated that with this technique it is possible to measure Raman spectra of different layers in a multilayered sample.
There are three different DIRS techniques. Each one exploits a different physical principle and measurement variable to select the signal from deeper layers: Spatially Offset Raman Spectroscopy (SORS) [1], exploits the variation of the penetration depth in CW regime with respect to the source detector distance, Frequency Offset Raman Spectroscopy (FORS) [2], exploits the variation of optical properties with wavelength and Time Domain Diffuse Raman Spectroscopy (TD-DIRS) [3], exploits the link between the time-of-flight of photons and their penetration depth in the material.

In our work we focused on TD-DIRS with the aim of determining its depth probing with respect to other measurement variables such as time, source detector distance and optical properties of the sample.
For this reason, in the first part of the work, described in section 2, we extended an existing description for Diffuse Raman, based on the Diffusion Approximation of the Radiative Transfer Equation [4], to derive a model for the calculation of the average generation depth of detected Raman photons with respect to their detection time.
We used then a system for TD-DIRS, described in section 3, with a spectrometer which exploits a single pixel camera and the compressive sensing approach to retrieve both a spectrum and its temporal evolution on a sub-nanosecond scale. This system has been improved with the addition of a new operation mode to make the alignment more precise and by the integration of all the program code needed to obtain and reconstruct a measure in a unique software which allows a quasi-real time monitoring of the instrumentation.
Finally, in section 4, the experimental measurements obtained from this system have been an-

alyzed and compared with our theoretical calculations developed in section 2.

2. Theoretical Elements

Before facing the experimental work we dealt with some theoretical elements in order to better understand the physics underlying Diffuse Raman Spectroscopy.
We started with the study of a theoretical model which describes the generation and propagation of Raman photons inside a turbid medium given an excitation light source $q(\vec{r},t)$ [4]. This model is based on two coupled Diffusion Equations: one for the fluence $\Phi(\vec{r},t)$ of photons injected in the material, the other for the fluence $\Phi_e(\vec{r},t)$ of Raman photons generated by those injected photons.

$$\begin{cases} \left(\frac{1}{v}\frac{\partial}{\partial t} - D\nabla^2 + \mu_a\right)\Phi(\vec{r},t) = q(\vec{r},t) \\ \left(\frac{1}{v_e}\frac{\partial}{\partial t} - D_e\nabla^2 + \mu_{ae}\right)\Phi_e(\vec{r},t) = q_e(\vec{r},t) \end{cases}$$

These two equations deal with two different wavelengths: λ for injected photons and λ_e for Raman photons. Note that, because of the dependence on the wavelength of refractive index n, absorption coefficient μ_a and scattering coefficient μ_s', the diffusion coefficient $D = 1/3\mu_s'$ and the light propagation speed $v = c/n$ assume different values in the two equations. The coupling term in the two equations is the source term for Raman light which depends on the fluence of excitation light. It is calculated as:

$$q_e(\vec{r},t) = \mu_{sR}\Phi(\vec{r},t)$$

with μ_{sR} a coefficient to consider the probability of Raman scattering.
We solved these equations in the case of a point-like instantaneous injection source and a semi-infinite homogeneous medium obtaining the reflectance $R_e(\rho,t)$ of the Raman signal we detect, since this quantity will be useful in a following step.
At this point, taking inspiration from reference [5], we developed an approach to calculate the probability density function $f(z,t)$ of detected Raman photons with respect to their generation depth z and detection time t. This function will allow us to calculate the average generation depth of detected Raman photons z_{avg}.

Our approach consists in isolating the contribution $\mathrm{d}R_e$ of the Raman photons generated in an infinitesimal layer $\mathrm{d}z$ at depth $\bar{z}$ to the total reflectance R_e. In fact, the probability density function we are looking for can be calculated as:

$$f(z,t) = \frac{1}{R_e(\rho,t)}\frac{\mathrm{d}R_e(\rho,t;\bar{z}=z)}{\mathrm{d}z}$$

To implement our approach we limited the source term of the second Diffusion Equation to a depth $\bar{z}$ with the multiplication by a delta function

$$q_e(\vec{r},t) = \mu_{sR}\Phi(\vec{r},t)\delta(z-\bar{z})$$

and we solved the system of equations as we did for the semi-infinite medium.
The resulting $f(z,t)$ can be expressed as:

$$f(z,t) = \frac{\int_0^t \frac{\exp\{\mu_{sR}vt'\}}{\sqrt{t'(t-t')}}\left[\exp\left\{-\frac{(z-z_S)^2}{4Dvt'}\right\} - \exp\left\{-\frac{(z+z_S+2z_E)^2}{4Dvt'}\right\}\right]\times}{\int_0^{+\infty}\int_0^t \frac{\exp\{\mu_{sR}vt'\}}{\sqrt{t'(t-t')}}\left[\exp\left\{-\frac{(z'-z_S)^2}{4Dvt'}\right\} - \exp\left\{-\frac{(z'+z_S+2z_E)^2}{4Dvt'}\right\}\right]\times} \\ \times\left[\exp\left\{-\frac{(-z)^2}{4Dv(t-t')}\right\} - \exp\left\{-\frac{(z+2z_E)^2}{4Dv(t-t')}\right\}\right]\mathrm{d}t' \\ \times\left[\exp\left\{-\frac{(-z')^2}{4Dv(t-t')}\right\} - \exp\left\{-\frac{(z'+2z_E)^2}{4Dv(t-t')}\right\}\right]\mathrm{d}z'\mathrm{d}t'$$

where z_S is the depth of the source and z_E the extrapolated boundary according to Extrapolated Boundary Conditions.
The behavior of $f(z,t)$ is shown in figure 1.

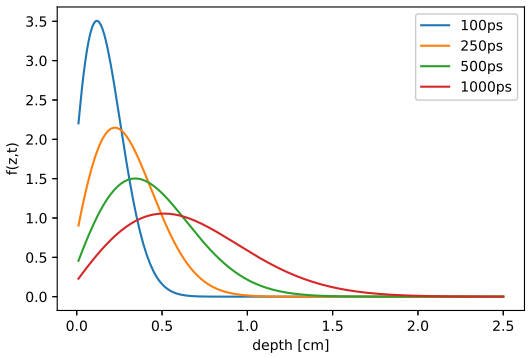

Figure 1: Probability density function $f(z,t)$ for $\mu_a = 0.1\mathrm{cm}^{-1}$ and $\mu_s' = 10\mathrm{cm}^{-1}$

From the probability density function it is then easy to calculate the average generation depth of detected Raman photons with

$$z_{avg}(t) = \langle z\rangle(t) = \int z f(z,t)\mathrm{d}z$$

The result is shown in figure 2.
As expected, a higher time-of-flight of the photons yields a higher generation depth. This justifies the experimental observations that by time

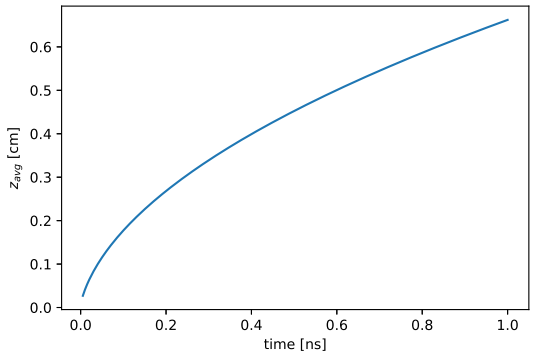

Figure 2: Average generation depth of detected Raman photons with respect to detection time for $\mu_a = 0.1\text{cm}^{-1}$ and $\mu_s' = 10\text{cm}^{-1}$

gating it is possible to select the signal coming from deep layers and obtain the Raman spectrum of different layers in our sample. Furthermore, now we can quantify the depth of each layer according to the selected time gate.
Thanks to these new calculations, it has been possible also to simulate a Diffuse Raman measurement of a bilayer medium. In fact, the signal for the top layer ($z < d$) and the bottom layer ($z > d$) can be respectively calculated as:

$$R_e^{TOP}(\rho, t) = R_e(\rho, t) \int_0^d f(z, t)\mathrm{d}z$$

$$R_e^{BOTTOM}(\rho, t) = R_e(\rho, t) \int_d^{+\infty} f(z, t)\mathrm{d}z$$

Nevertheless, we have to remark that the calculations we developed involve some approximations: firstly we considered the same values of optical properties for wavelength λ and λ_e; secondly, we considered the optical properties as constant in the whole medium as if it were an homogeneous medium. Since these approximations are far from reality we will expect that our model will not be much precise.

3. TD-DIRS System

In this section we present the instrumentation for TD-DIRS that has been improved and used during this thesis work.
At a very high level it is possible to identify four main parts in our system:

- a laser source which provides the light to excite the sample;
- illumination optics to deliver light to the surface of the sample;
- collection optics to collect light from the sample and select only Raman scattered photons;
- a spectrometer which allows the measurement of the Raman spectrum.

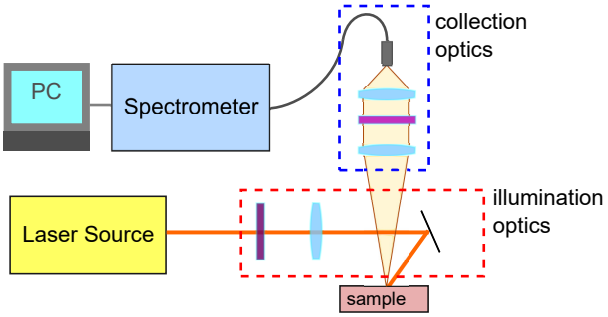

Figure 3: Schematic drawing of the instrumentation

The laser source we used is a custom made Ti:Sapphire laser which can work both in continuous wave (CW) or in active mode-locking (ML) regime with a tunable wavelength from 700 nm to 860 nm. We measured a maximum power achievable of 1.95 W in CW and 0.76 W in ML, a spectral bandwidth less than 0.1 nm and a pulse duration of 90 ps.
The illumination optics include a band pass filter (BP780-10, Thorlabs) to clean the laser beam from other wavelengths different than the excitation one (780 nm) and either a lens, to focus the laser beam in a small spot thus obtaining a point illumination scheme, or an axicon (AX255, Thorlabs), to spread the laser light over a ring of radius 5 mm centered on the collection point thus obtaining a ring illumination scheme.
The collection optics consist of a simple optical system to collect light from the surface of the sample with a non-contact approach and couple it in a round to linear fiber bundle (BFL200LS02, Thorlabs) directed to the spectrometer. Inside the optical system there is also a long pass filter (FELH800, Thorlabs) which removes the Rayleigh scattered light and leaves only the Raman photons.
The spectrometer is the most interesting part of the instrumentation. Its design, inspired by reference [6], is based on a single-pixel camera built with a digital micromirror device (DMD - DLP6500, Texas Instruments) and a Time Correlated Single Photon Counting (TCSPC) detection so to collect both the spectrum and its temporal evolution. Its optical scheme is repre-

sented in figure 4.

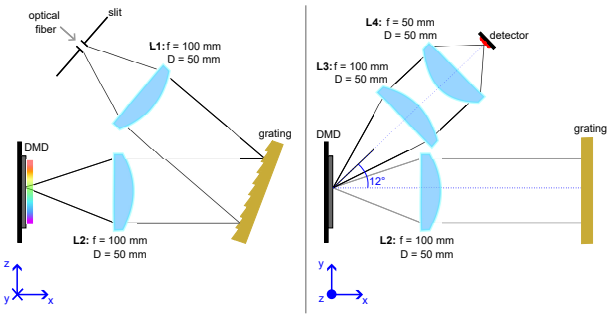

Figure 4: Scheme of the spectrometer

According to the patterns created on the DMD, the spectrometer can operate in three different modes.

Monochromator mode: each pattern activates a line of micromirrors perpendicular to the dispersion direction of the spectrum so that a raster scan of the spectrum is performed;

Multiplex mode: Hadamard bases are exploited to generate striped patterns and send multiple wavelengths to the detector at the same time. This allows having a higher collection efficiency than in the monochromator mode, since for each pattern 50% of the spectrum is sent to the detector. However the measurements need a reconstruction process in which the measurements vector $\mathbf{x}$ is multiplied by the Hadamard matrix H in order to obtain the original spectrum $\mathbf{y} = H^{-1}\mathbf{x} = H\mathbf{x}$ (as $H^{-1} = H^T = H$). Actually we use a more robust reconstruction algorithm based on least square minimization $\min \|\mathbf{y} - H\mathbf{x}\|_2$ which gives better results;

Imaging mode: this is the new mode added to improve the spectrometer. In this mode we exploit the imaging capability of the single-pixel camera [7] to capture the image of the light spot on the DMD. This is very useful during the alignment phase of the spectrometer in which the size of this spot has to be minimized in order to reach the best spectral resolution. The patterns used in this mode are also derived from an Hadamard basis set, however, each Hadamard basis, instead of being directly projected on the DMD in a striped pattern as in multiplex mode, is reshaped in a square matrix so to create a set of patterns made of rectangles. The measurement then needs a reconstruction process (such as that of the multiplex mode) in order to obtain the original image.

All the instrumentation is controlled by a unique software which allows one to set up, run and reconstruct a measurement. This is also the product of the improvement given at the system during our work. In fact, we integrated the existing program code to handle the DMD (using DLL libraries) and the Python code to reconstruct measurements (using Python/C APIs) in a program called TRS used in many laboratories at Physics Department of Politecnico di Milano. The software has nearly real time capabilities showing a refresh rate of 0.3 Hz, good enough for the alignment phase of the spectrometer. Moreover, we have simplified the use of the system since only one software is now needed instead of three.

We finally characterized the improved system, in particular the spectrometer, measuring a spectral range of 60 nm (800 cm^{-1}), a spectral resolution of 0.8 nm and a power efficiency, defined as the ratio between the power at the detector and the power at the input of the spectrometer, of 4.3%.

4. Experimental Measurements

Our system produces measurements of the Raman spectrum and its distribution of photon arrival times. To visualize a measurement, we use a 2D map in which the y axis is for the spectrum while the x axis is for the time, like that in figure 5. By summing the signal over a time gate one obtains the Raman spectrum of the sample. Selecting different time gates enables the visualization of the Raman spectrum of different depths in the sample. By slicing the 2D map in the horizontal direction it is possible to view the temporal behavior of a specific Raman shift.

After having verified the correct functioning of the spectrometer with the measurements of different samples for which the Raman spectrum was known (marble/calcite $CaCO_3$, hydroxyapatite $Ca_{10}(PO_4)_6(OH)_2$, silicone PDMS), we proceeded in measuring bilayer samples in order to demonstrate the capability of our TD Diffuse Raman Spectrometer in doing depth profiling of multilayered materials.

Our bilayer samples consisted of silicone slabs with different scattering coefficients ($\mu_s' = 5$ cm^{-1}, $\mu_s' = 10$ cm^{-1}, $\mu_s' = 15$ cm^{-1}) and different thicknesses (0.5 cm, 1 cm) put on top of a marble block. Each measurement was repeated with both the point illumination scheme and

the ring illumination scheme. The spectrometer was used in the multiplex mode with a set of 256 Hadamard bases, a single pattern exposition time of 0.5 s and 15 repetitions of a single measurement were taken so that the total measurement time was 32 minutes.
These measurements allowed us to have a complete picture of the effect of source detector distance, scattering coefficient of the top layer and thickness of the top layer on the final result of the measurement. In particular, we observed that increasing the source detector distance, the intensity of the detected signal decreases and the weight of the bottom layer spectrum with respect to the top one is increased. Increasing the scattering coefficient of the top layer, instead, makes the spectrum of the top layer become more predominant with respect to the spectrum of the bottom layer, as predicted also by our theoretical model. Increasing the thickness of the top layer, the signal of the top layer is unchanged while the signal of the bottom layer is subjected to a decrease in intensity.
However, the most important analysis done on these bilayer measurements is about the effect of time gating. We chose three time gates with the same duration of 200 ps, as shown in figure 5: an early gate comprising the rising edge of the signal, a middle gate at the center of the pulse (225 ps after the starting point of the first gate) and a late gate placed on the tail of the temporal curve (450 ps after the starting point of the first gate).

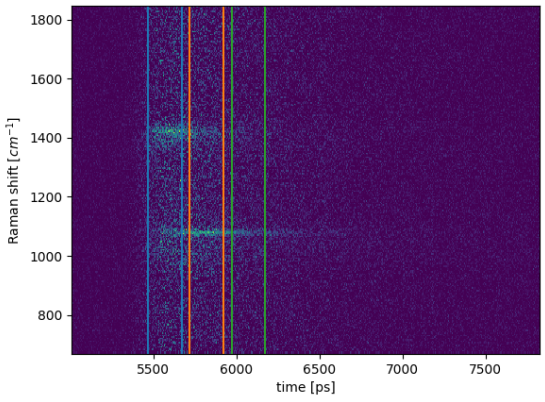

Figure 5: Example of 2D map obtained from a measurement and different time gates chosen for the analysis

The corresponding Raman spectrum for each time gate in a measurement of a bilayered sample with PDMS top layer $\mu_s' = 5$ cm^{-1}, thickness 0.5 cm and point illumination scheme is shown in figure 6. It is possible to note that our TD-

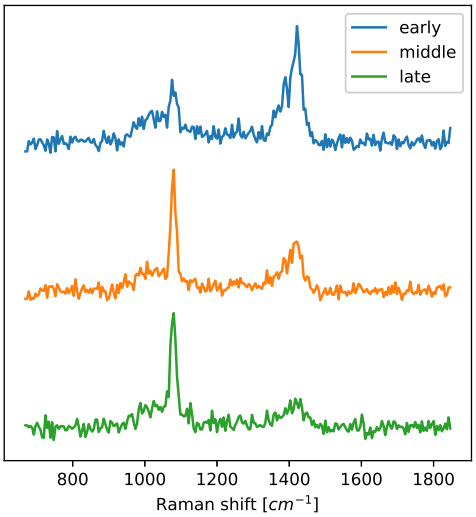

Figure 6: Raman spectra of different time gates

DIRS system is actually capable of isolating the Raman signal coming from different depths of the sample thanks to time gating. In fact, the spectrum obtained with the early time gate is characterized mostly by the contribution of the Raman peak of PDMS (top layer) at 1400 cm^{-1} while in the spectrum obtained with the late time gate we can see mostly the contribution of the Raman peak of marble (bottom layer) at 1080 cm^{-1}.
Moreover, with this analysis we can highlight a big advantage of our system: thanks to the TCSPC acquisition we can apply the time gating during post-reconstruction of the measurements thus allowing a free choice of the gate position and duration. In principle, it is possible to optimize the time gate in order to obtain a complete isolation of the top layer and bottom layer Raman spectra.
As a last analysis on these measurements, we did a comparison with the previsions of the developed theoretical model. In particular, we compared the temporal evolution of top layer and bottom layer signals obtained experimentally and simulated with the theoretical model of section 2. The signal of the simulations has been convolved with the temporal response of our in-

strumentation and superimposed to the corresponding experimental measurement as shown in figure 7.

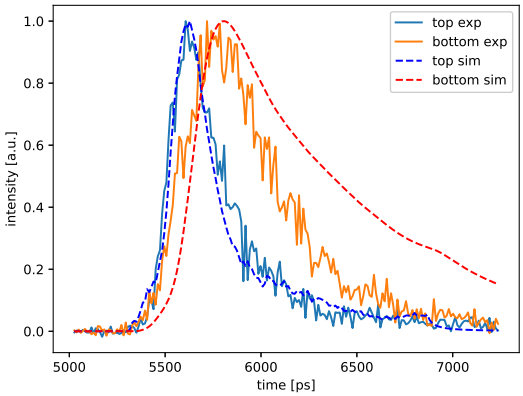

Figure 7: Comparison between an experimental measurement and a simulation. Parameters: $\mu_s' = 10\text{cm}^{-1}$, thickness = 0.5 cm, point illumination (each temporal curve has been normalized to remove differences in peak intensities)

It is possible to note that the simulation reproduce well the time evolution of the experimental data. In fact, in both cases we see the presence of a delay between the bottom layer signal and the top layer one and of a time in which the signal of the bottom layer starts to prevail with respect to the signal of the top layer. However, the simulation gives a longer delay and a higher tail in the bottom signal than those observed experimentally. This could be due to the approximations we did in the theoretical calculations. In particular, since in our simulation the optical properties in the whole medium are equal to those of the top layer, we are not considering that actually marble has a much higher absorption coefficient than that of the PDMS top layer, so a steeper decrease of the temporal curve in the experimental measurement with respect to the simulation is reasonable.
From this comparison, that has been repeated for every measurement, we can affirm that our developed theoretical model could be a plausible one since, despite the quantitative differences, it predicts the correct behavior of the Raman signal. Nevertheless, we cannot declare its validity since our experimental data are not sufficient.

5. Conclusions

In conclusion, we can say that all the works faced during this thesis produced some interesting and new results.
In fact, studying a theoretical model for the description of Diffuse Raman, we were able to find a new approach to calculate the probability density function of detected Raman photons with respect to their generation depth and detection time and to determine the average generation depth of detected Raman photons with respect to their detection time. Moreover, with this model we managed to obtain the simulation of a measurement on a bilayered sample. The results obtained are qualitatively consistent with our expectations and experimental observations.
We were able to bring some improvements at the TD-DIRS system making easier its usability and increasing its precision. In particular, we introduced a new operation mode (imaging mode) and we integrated all the program code needed to set up, run and reconstruct a measure in a single software with a nearly real time response (refresh rate 0.3 Hz). Both these functions permitted to reach a better alignment of the spectrometer and a resolution of 0.8 nm.
Thanks to the experimental measurements on bilayered samples, we managed to observe the effect of some experimental variables (source-detector distance, scattering coefficient, thickness of the top layer) on the measurement itself and to demonstrate the depth probing capability of TD-DIRS by means of time gating. Then, by comparing the experimental measurements with the simulations obtained from the theoretical model, we could affirm the plausibility of our theoretical model.
In light of these results we can identify some future perspectives. The first one is the validation of our theoretical model with Monte Carlo simulations or/and better experimental measurements and eventually its refinement by removing some approximations in order to simulate more realistic situations. The second one concerns the system that could be further improved with the aim to increase the collected signal thus allowing to obtain better measurements and eventually decrease the measurement time. The ultimate goal is then the application of our system to in vivo measurements.

References

[1] Sara Mosca, Claudia Conti, Nick Stone, and Pavel Matousek. Spatially offset raman spectroscopy. *Nature Reviews Methods Primers 2021 1:1*, 1:1–16, 3 2021.

[2] Sanathana Konugolu Venkata Sekar, Sara Mosca, Andrea Farina, Fabrizio Martelli, Paola Taroni, Gianluca Valentini, Rinaldo Cubeddu, and Antonio Pifferi. Frequency offset raman spectroscopy (fors) for depth probing of diffusive media. *Optics Express*, 25, 3 2017.

[3] A. Pifferi, E. Turbin, F. Martelli, G. Valentini, R. Erdmann, S. Konugolu Venkata Sekar, S. Mosca, S. Tannert, T. Binzoni, W. Zuschratter, and Y. Prokazov. Time domain diffuse raman spectrometer based on a tcspc camera for the depth analysis of diffusive media. *Optics Letters, Vol. 43, Issue 9, pp. 2134-2137*, 43:2134–2137, 5 2018.

[4] Fabrizio Martelli, Tiziano Binzoni, Sanathana Konugolu Venkata Sekar, Andrea Farina, Stefano Cavalieri, and Antonio Pifferi. Time-domain raman analytical forward solvers. *Optics Express*, 24, 9 2016.

[5] Fabrizio Martelli, Tiziano Binzoni, Antonio Pifferi, Lorenzo Spinelli, Andrea Farina, and Alessandro Torricelli. There's plenty of light at the bottom: statistics of photon penetration depth in random media. *Scientific Reports 2016 6:1*, 6:1–14, 6 2016.

[6] Pascal Berto, Camille Scotté, Frédéric Galland, Hervè Rigneault, and Hilton B. de Aguiar. Programmable single-pixel-based broadband stimulated raman scattering. *Optics Letters*, 42:1696, 5 2017.

[7] Marco F. Duarte, Mark A. Davenport, Dharmpal Takbar, Jason N. Laska, Ting Sun, Kevin F. Kelly, and Richard G. Baraniuk. Single-pixel imaging via compressive sampling: Building simpler, smaller, and less-expensive digital cameras. *IEEE Signal Processing Magazine*, 25:83–91, 2008.